Asian Journal of Chemistry; Vol. 36, No. 2 (2024), 393-403

ASIAN JOURNAL OF CHEMISTRY

https://doi.org/10.14233/ajchem.2024.30963

Effect of Azo Dye Red 2G on Human Gamma Globulin using Multi-Spectroscopic and Docking Studies

S. GAYATHRI and S. BAKKIALAKSHMI*

Department of Physics, Annamalai University, Annamalai Nagar-608002, India

*Corresponding author: E-mail: bakkialakshmis@rocketmail.com

Received: 27 November 2023; *Accepted*: 31 December 2023; *Published online*: 31 January 2024; AJC-21527

The study explored the binding interaction between human gamma globulin (HGG) and the synthetic azo dye red 2G (R2G) using spectroscopic techniques and molecular docking studies. The binding effects were identified through UV-visible, fluorescence and FT-IR spectroscopies. The quenching mechanism was found to be static, resulting in the formation of a stable bioconjugate, as determined by Stern-Volmer analysis. The binding distance between R2G and the tryptophan residue of HGG was studied using the Forster resonance energy transfer (FRET) theory. The study also found significant modification in the amide FTIR frequencies correlating to variation in the secondary α-helical structures of HGG at the HGG-R2G complex interface. The binding affinity scores of the protein HGG with the dye were determined using molecular docking. Biophysical techniques, such as turbidity measurements and field emission scanning electron microscopy (FESEM), were used to understand the mechanism of R2G-induced amyloid aggregation in HGG at pH 2. Additionally, the study investigated the potential cytotoxic effects of red 2G on human THP-1 monocytes *via* an MTT assay. The effects of food colorants on biological macromolecules were studied and it was found that a higher concentration of red 2G has toxic potential to human THP-1 monocytes.

Keywords: Azo dye, Human gamma globulin, Fluorescence, Docking studies, Turbidity, Cytotoxicity.

INTRODUCTION

Blood plasma is a heterogeneous fluid consisting of various proteins, enzymes, hormones and other molecules that are essential for the regulation of the body's physiological processes [1]. Among these components, proteins are the most abundant, with an average concentration of 7.2 g/dL in normal human plasma. These proteins have diverse functions, such as maintaining osmotic pressure, transporting lipids and metals and regulating blood coagulation and immune response [2,3].

Immunoglobulin G (IgG), sometimes referred to as human gamma globulin, is a vital component of the human immune system that is produced by the immune system's plasma cells and lymphocytes [4]. It is a member of the immunoglobulin protein family and is essential to the body's defence against infections. One of the main types of antibodies present in blood and other body fluids is gamma globulin. Specialized proteins called antibodies are able to identify and attach to particular foreign things including viruses, bacteria and poisons [5]. Because these antibodies are frequently isolated from other blood proteins in the gamma fraction during laboratory techniques, the name "gamma globulin" is used [6].

Azo dyes are a major class of synthetic organic dyes known for their versatility and chemical stability. They contain one or more azo groups (–NN–) connected to aromatic rings and the majority of commonly used dyes belong to this class [7,8]. Artificial food colour additives, commonly called food dyes, are composed of a complex mixture of chemicals that are frequently derived from highly toxic sources such as coal tar or petroleum. These chemicals have been associated with various adverse health effects in humans, including carcinogenic, mutagenic and teratogenic effects. Furthermore, they have been linked to numerous diseases, disorders and mutations, making it crucial to consider their potential health risks when assessing the safety of food products [9].

Red 2G (R2G) is a synthetic red azo dye that is commonly used in the food industry for its ability to impart a vivid red hue to a variety of food products. It is a disodium salt of 5-acetylamino-4-hydroxy-3-(phenylazo)naphthalene-2,7-disulphonate, with a molecular weight of 509.4 g/mol and

soluble in water but partially soluble in glycerol. R2G is frequently added to red wine, yogurts, drinks, red sausages, jams and deli meats to obtain colours ranging from peach red to blood-red [10]. Red 2G, an unapproved colorant used in food, has the potential to be metabolized into aniline, a harmful chemical, within the gastrointestinal tract. This raise concerns that red 2G may interfere with blood proteins and increase harmful risk [11]. Red 2G, used as a food colorant, has been detected in 43 food products that are frequently consumed by children and adults [9]. Dye-macromolecule interaction is a crucial aspect of the safety and toxicological assessment of dyes [12]. The binding of small molecules to proteins can cause significant modifications in the protein's structure, which is critical for comprehending the biological functionality and action mechanism of the protein [13].

The investigation of the binding mechanism of R2G-HGG using fluorescence spectroscopy has not yet been reported in the literature. This work aimed to probe the molecular interaction of red 2G (R2G) dye with human gamma globulin (HGG) using multispectroscopic techniques and auto dock-based molecular modelling. The spectroscopic techniques revealed the kind of interaction that takes place between R2G and HGG. The binding mode and binding constant can also be evaluated using fluorescence spectroscopic techniques. The conformational change in the secondary structure of HGG due to the presence of red 2G was detected by FTIR. Molecular docking revealed the binding forces and the amino acid residues involved in the interaction. Amyloid fibril formation was characterized using spectroscopic techniques to understand the molecular mechanism of HGG aggregation by R2G. Furthermore, the *in vitro* cytotoxic effect of red 2G against the human monocyte THP-1 cell line was also studied.

EXPERIMENTAL

Human gamma globulin (purity ≥ 90%), red 2G (dye content, 85-95%) and 1.0 M phosphate buffer (pH 7.4) were procured from Sigma-Aldrich, USA. All other reagents used in this study were of analytical grade and the double distilled water was used throughout the study.

Stock solution preparation: Human gamma globulin (HGG) stock solution (1×10^{-5} M) was prepared in 1 M phosphate buffer (*i.e.* physiologic pH 7.4). The concentration of HGG was estimated spectrophotometrically using an extinction coefficient of 11,000 M^{-1} cm^{-1} at 278 nm. R2G dye (1×10^{-4} M) was prepared in double distilled water. All protein and dye stock solutions were also prepared freshly.

UV-visible spectroscopic analysis: Absorption measurements were carried out using UV-visible Spectrophotometer Shimadzu-UV 1800 model. The optical properties of the solutions were analyzed using a quartz cell with an optical pathlength of 1 cm and the spectra were recorded over a range of 200-800 nm.

Steady state fluorescence spectroscopy: A RF-5301PC model of Shimadzu Corporation spectrofluorimeter was utilized to acquire the steady-state fluorescence spectra data. This study, utilized intrinsic fluorescence spectroscopy to analyze human gamma globulin samples containing varying concentrations of R2G. The emission wavelengths were scanned between 250 nm to 500 nm with an excitation wavelength of 278 nm, while both the excitation and emission slit widths were maintained at 5.0 nm.

In order to remove the inner filter and re-absorption, $F_C = F_{ob} e^{\frac{A_{ex} + A_{em}}{2}}$, was used to correct all of the fluorescence data. The F_{ob}, the measured fluorescence intensity and the corrected fluorescence intensity (F_c) respectively, the absorption of dye at the excitation and emission wavelengths is represented by the symbols A_{ex} and A_{em}, respectively

Synchronous fluorescence spectroscopy: Synchronous fluorescence spectra of the protein HGG, with the presence of mounting R2G concentration, were recorded using RF-5301PC spectrofluorimeter. The concentration is same as specified in the fluorescence measurements. The objective was to evaluate alterations in the microenvironment surrounding tyrosine and tryptophan amino acid residues present in biomolecules. The changes were measured using fixed $\Delta\lambda$ values of 15 nm and 60 nm.

Time-resolved fluorescence analysis: Fluorescence lifetime intensity decay measurements were carried out using Fluorolog FL3-11 spectrofluorometer equipped with time-correlated single photon counting method with a nano-LED source (Jobin Yvon) used as an excitation source.

FT-IR analysis: FT-IR spectra of HGG and HGG-R2G samples in the range from 4000 to 400 cm^{-1} were recorded using the Perklin-Elmer spectrometer. To minimize the impact of solvent interference on the measurement results, ethanol was used instead of H_2O as solvent in the FTIR acquisition process for preparing the sample.

Turbidity analysis: The turbidity assay measurements were carried out to probe the aggregation in HGG induced by R2G. The treated and untreated samples were measured using UV-visible spectrophotometer Shimadzu-UV 1800 by taking absorbance at 650 nm. In brief, HGG (2 mg) dissolved in 10 mL of glycine-HCl buffer at pH 2.0 and then different concentrations of R2G (0.0 to 2.0 Mm) were treated with 0.2 mL of HGG, finally the samples were incubated overnight at room temperature. The turbidity was also measured in samples containing R2G alone at pH 2.0.

FESEM analysis: HGG aggregates were subjected to surface morphology analysis using the CARL ZEISS–SIGMA 300 FESEM, a field emission scanning electron microscope. 50 µL of sample containing HGG (0.2 mL) treated with red 2G (1.8 mM) incubated overnight at pH 2.0 and applied on the surface of conductive carbon tape on the aluminium stub, followed by air-dried at ambient temperature for 24 h. After that the surfaces were vacuum-sputter coated with a thin layer of chromium. The chromium-coated samples were placed on FESEM with an operating voltage of 0.02-20 kV and images were captured.

Molecular docking: Auto Dock 1.5.6 software from the SWISS Model repository (http://autodock.scripps.edu/) was used for the molecular docking of R2G to HGG.

Protein structural preparation: For docking simulations, the three-dimensional coordinates of HGG were extracted from its X-ray crystal structure (PDB ID:1AJ7 resolved at 2.20 Å) available in the RCSB database. Protein X-ray crystal structure refinement was performed by removing non-essential water molecules and optimizing the polar hydrogen atoms and Kollman charges were assigned using Auto Dock. A 40 Å × 40 Å × 40 Å grid box was generated as the HGG active-site cavity was embedded and the default grid spacing is 0.375.

Ligand structural preparation: The two-dimensional R2G crystal structure (CID:164825) was obtained from the National Center for Biological Information (PubChem database). Using Auto Dock Tools version 1.5.6, nonpolar hydrogens were combined, Gasteiger charges were applied, aromatic carbons and rotatable bonds were tallied, TORSDOF was determined and the data were transformed into the PDBQT file format, which represents the protein data bank, partial charge and atom type.

Docking protocol: The flexible ligand-protein docking process was carried out using the Lamarckian genetic algorithm (LGA). HGG was considered rigid and the input torsion roots of the flexible R2G ligand were set. Performed 10 runs of a genetic algorithm with default settings, using a maximum of 2.5 million energy assessments and a population size of 150, with a maximal limit of 27,000 generations, other parameters were left at their default settings. The lowest binding energies of the docked complexes were analyzed and stable conformations were visualized using PYMOL and BIOVIA Discovery Studio.

Cell viability MTT assay: The THP1 cell line, derived from a human monocytic cell line and obtained from the National Centre for Cell Science (NCSS), Pune, India was cultured in Roswell Park Memorial Institute medium (RPMI) supplemented with 10% fetal bovine serum and 1% antibiotic-antimycotic solution (Hi-Media Laboratories Mumbai, India). The experiment involved seeding cells in 96-well plates at a density of 50×10^3 cells per well, followed by an overnight incubation at 37 ºC in 5% CO_2 atmosphere.

The cytotoxic impact of red 2G on the THP-1 human monocyte cell line was assessed using the MTT assay, which utilizes 3-(4,5-dimethylthiazol-2-yl)-2,5-diphenyltetrazolium bromide. The assay measures cell viability by evaluating reductive activity. After seeding, THP-1 cells were treated with R2G at doses ranging from 500 to 2500 µg/mL. They were then incubated for an additional 48 h at 37 ºC in 5% CO_2. Following the application of azo dye R2G, each well received 20 µL of MTT solution (0.5 mg/mL in PBS), which was then incubated for 3 h. After carefully discarding the supernatant, 100 µL/well of DMSO solvent was added to dissolve the formazan crystals. Doxorubicin-treated cells with a concentration of 6.43 µg/mL served as a positive control while untreated cells with only medium acted as the negative control, displaying the highest viability. The optical density at 570 nm was measured using a spectrophotometer or an ELISA reader. Using nonlinear regression sigmoidal dose-response analysis and logarithmic transformation of the R2G concentration, the IC_{50} value was determined. The viability percentage was determined by applying the OD value to the following formula:

$$\text{Cell viability (\%)} = \frac{\text{Opetical density of sample}}{\text{Optical density of negative control}} \times 100$$

RESULTS AND DISCUSSION

Absorption spectroscopic studies: Fig. 1a displays the UV-visible absorption spectra of R2G without HGG and with HGG. As illustrated in Fig. 1a, the addition of R2G causes the absorbance of cystine (*i.e.* disulfide bonds) to increase some extent, which in turn causes the absorbance of tryptophan and tyrosine, two aromatic amino acids, and the absorbance of HGG reaches a plateau at 278 nm. The absorption intensity of the R2G-HGG samples increases with higher R2G concentrations and there are no significant changes in the peak location.

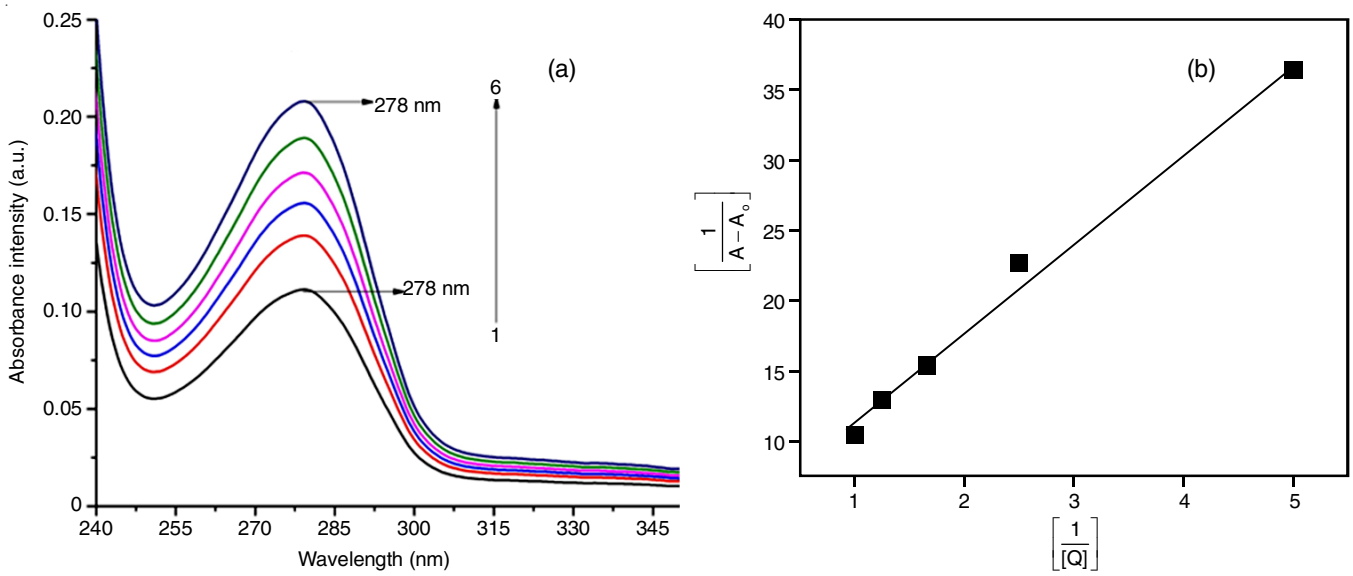

Fig. 1. (a) UV-vis absorption spectra of human gamma globulin with different concentrations of red 2G (1) 0.0, (2) 0.2, (3) 0.4, (4) 0.6, (5) 0.8 & (6) 1.0×10^{-4} (mol L^{-1}), (b) The plot of $1/A–A_o$ *versus* 1/[Q] for HGG with red 2G dye

These results indicated that the microenvironment around the amino acid residues in HGG remains unchanged upon the interaction with R2G and a lack of significant conformational changes in the protein structure [14]. An increase in the absorbance of HGG is due to the formation of a ground-state combination between red 2G and HGG [15].

The Benesi-Hildebrand (B-H) plot was formed using the changes in absorbance intensity of HGG in the presence of R2G. The linear dependence of the plots of $1/(A-A_o)$ *versus* 1/[R2G], as shown in the inset of Fig. 1b, confirms the formation of a well-defined 1:1 complex (HGG-R2G) in the ground state. The binding constants (K_a = 1.52 × 10^4 L mol^{-1}) have been calculated by dividing the intercept with the slope with linear regression coefficient R^2 = 0.99) were determined, demonstrating the moderate binding affinity of the R2G dye to HGG in the ground state [16].

Fluorescence quenching mechanism and determination of binding constant and binding sites: Fluorescence quenching mechanism is depicted to understand the binding behaviour based on the potential interaction between HGG and R2G. The spectrum of fluorescence can change due to changes in the surrounding environment around protein residues that contain aromatic amino acids. This phenomenon is often used to study the interactions between proteins and ligands and to gain a better understanding of the structural properties of biomolecules [17,18]. Therefore, the fluorescence quenching of HGG without and with red 2G was performed. The fluorescence intensities of HGG at pH 7.4 without and with red 2G after excitation at 278 nm are shown in Fig. 2a.

From Fig. 2a, it can be clearly seen that the HGG without red 2G showed maximum fluorescence at 337 nm, which is mainly due to tryptophan residues. These residues are highly sensitive to local polarity [19]. The data suggests that substance R2G is capable of inhibiting the intrinsic fluorescence of human gamma globulin. This is demonstrated by a gradual decrease in the protein's emission intensity as the concentration of R2G increases. The results indicated that R2G has a direct interaction with the chromophores of the gamma globulin protein. Moreover, there is no discernible alteration in the emission maximum, which implies that R2G has a limited impact on the environment surrounding the tryptophan components [20].

Using the Stern-Volmer equation (eqn. 1), the mechanism of fluorescence quenching was ascertained.

$$\frac{F_o}{F} = 1 + K_q \tau_o [Q] = 1 + K_{sv}[Q] \quad (1)$$

$$K_q = \frac{K_{sv}}{\tau_o} \quad (2)$$

The fluorescence intensities (red 2G) measured with and without a quencher are denoted by F_o and F, respectively. The interaction between HGG and R2G dye was investigated using a Stern-Volmer plot (Fig. 2b) and was found to have a high linear correlation coefficient (R^2 = 0.99). The quenching efficiency of R2G can be calculated using this graph (Fig. 2b) substance is more effective at quenching the fluorescence of macromolecule or protein if its K_{sv} value is higher. The K_{sv} coefficient for the present azo dyes was found to be 5.28 × 10^4 M^{-1}. A higher K_{sv} value indicates that R2G is more effective at quenching the fluorescence of HGG. The bimolecular quenching constant (K_q) can be calculated from the quenching constant, K_{sv} and τ_0, using eqn. 2. Dynamic quenching is typically characterized by a K_q value of approximately 1 × 10^{10} M^{-1} s^{-1}, which indicates a swift quenching process. However, the K_q value in dynamic quenching can be reduced by steric shielding that hinders the fluorophore from coming into contact with the quencher. In contrast, the static quenching happens when a fluorescent molecule and a quencher form a complex in the ground state, producing a non-fluorescent species. Higher K_q values are linked to static quenching and denote the strength of the interaction between the fluorophore and the quencher [21,22].

In the HGG-R2G interaction, the limiting dynamic diffusion rate constant is substantially smaller than the quenching rate

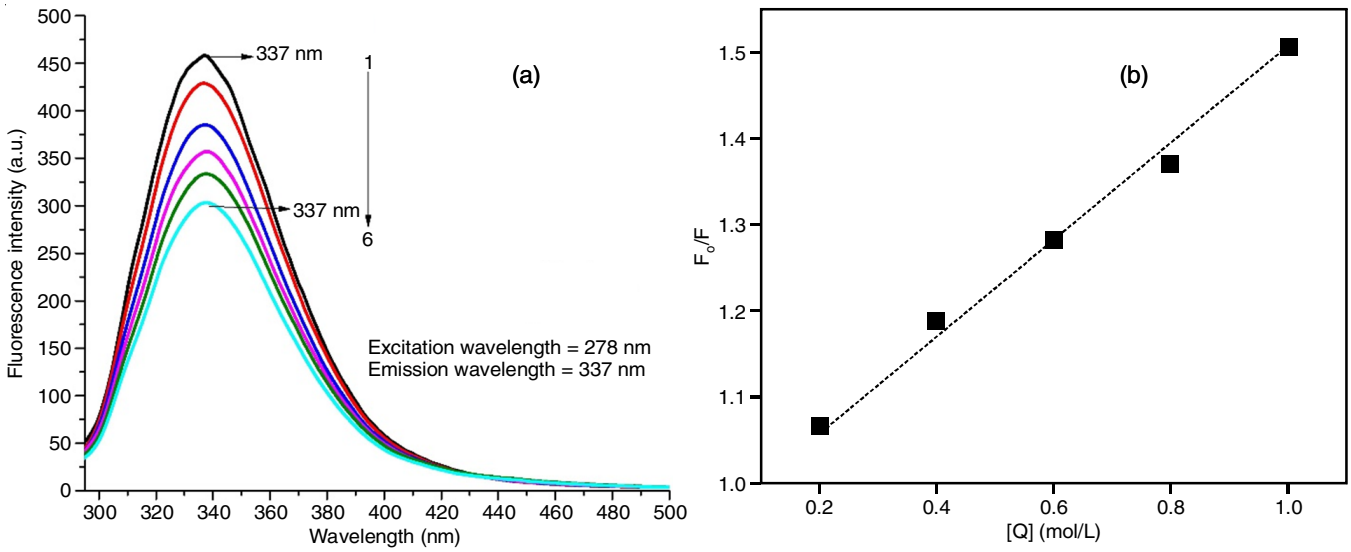

Fig. 2. (a) Steady-state fluorescence spectra of human gamma globulin with different concentrations of red 2G (1) 0.0, (2) 0.2, (3) 0.4, (4) 0.6, (5) 0.8 & (6) 1.0 × 10^{-4} M, (b) The Stern-Volmer plot for HGG with red 2G dye

constant. ($K_q = 3.34 \times 10^{13}$ M^{-1} s^{-1}), suggesting the existence of a static quenching mechanism that helps in the formation of stable R2G dye-HGG complexes [23].

Binding parameters: The binding affinity of ligand on the receptor can be evaluated using eqn. 3:

$$\log\left(\frac{F_o - F}{F}\right) = \log k_\alpha + n \log[Q] \quad (3)$$

A double logarithmic plot can be used to determine the binding constant (K_a) and the number of binding sites per globulin molecule (n) (Fig. 3). The plot shows a good linear fit (Fig. 3) depicting that the interaction mechanism between red 2G and human gamma globulin has an agreement with the above equation underlies the site binding model [24].

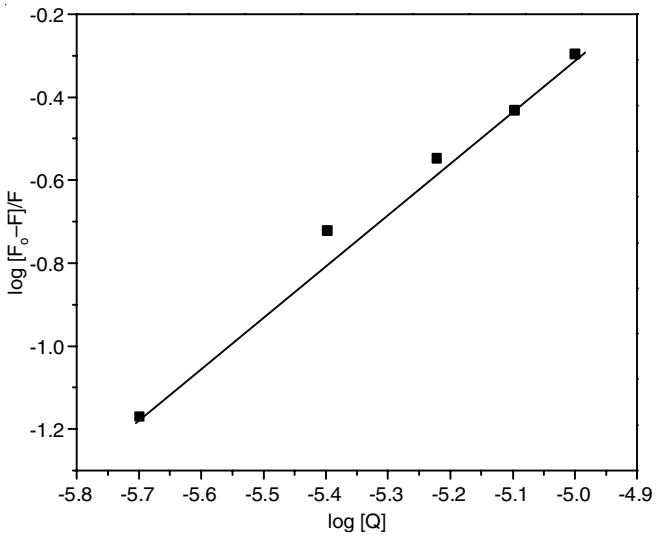

Fig. 3. Double logarithmic plot of human gamma globulin with red 2G

The calculated value of n = 0.96 from the double reciprocal curve reveals that the interaction system has a single independent binding site [25,26]. The value of K_a (Table-1) in the range of 10^4 M^{-1} generally signifies the moderate binding strengths, which is a close agreement with the reported literature of binding studies of ligands with protein [27]. The negative values of free energy (ΔG) support that the binding of azo dye to HGG is a spontaneous process [28].

TABLE-1
BINDING PARAMETERS OF HUMAN GAMMA GLOBULIN WITH RED 2G DYE

Quenchers	K_a (L mol^{-1})	n	R^2	S.D.
Red 2G	6.91×10^4	0.96	0.98	2.67

Synchronous spectroscopic studies: The synchronous fluorescence spectroscopy is a well-established analytical technique used to investigate the impact of ligands on the tertiary structure of proteins [29]. This method uses a fixed difference of 15 nm between the excitation and emission wavelengths to analyze the fluorescence of Tyr and Trp residues in proteins effectively.

From Fig. 4, it was observed that the fluorescence intensity of HGG decreased with the increasing concentration of R2G. This indicated that the binding of R2G with HGG caused the quenching of both Tyr and Trp residues in protein. The fluorescence intensity of Trp residues was found to be much stronger than that of Tyr residues.

However, the structure of both microregions remained unchanged despite the changes in fluorescence intensity. The finding suggests that R2G interacts with HGG, without affecting the maximum emission wavelength. This implies that the polarity around Trp and Tyr remains constant. The formation of HGG-R2G complexes has little influence on the microenvironment around the amino acid residues. However, it causes a decrease in fluorescence intensity. This observation confirms the idea of an interactive engagement between HGG and R2G, indicating the existence of an interaction between these two compounds [30].

Time resolved fluorescence spectroscopic studies: Time resolved lifetime studies are a powerful experimental technique that plays a crucial role in the investigation of various photophysical processes. By analyzing the decay of excited states

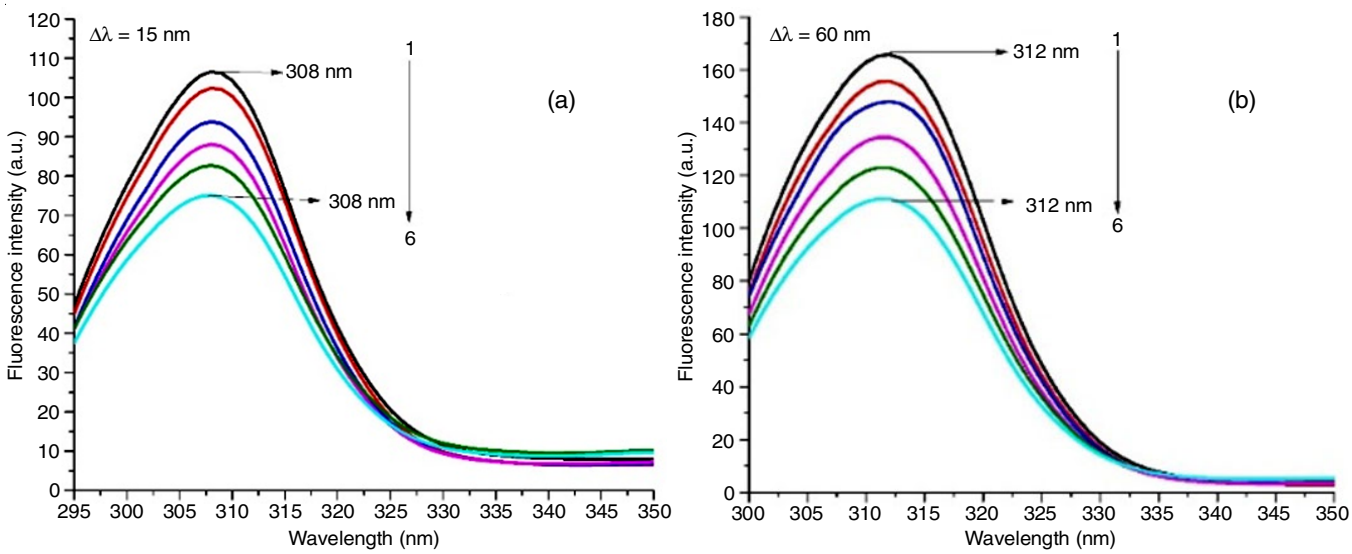

Fig. 4. Synchronous fluorescence spectra of human gamma globulin with red 2G at (a) Δλ = 15 nm and (b) Δλ = 60 nm

TABLE-2
FLUORESCENCE LIFETIME AND RELATIVE AMPLITUDES OF HUMAN GAMMA GLOBULIN WITH DIFFERENT CONCENTRATIONS OF RED 2G DYE

Concentration (M)	Lifetime (ns)			Average lifetime × 10^{-9} s	Relative amplitude			χ^2	Standard deviation × 10^{-11} s		
	τ_1	τ_2	τ_3		α_1	α_2	α_3		τ_1	τ_2	τ_3
HGG	0.93	2.11	6.15	1.77	37.64	59.74	2.62	1.20	6.49	3.71	18.34
HGG + R2G (0.4M)	0.86	2.05	6.63	1.67	42.24	55.07	2.69	1.20	4.27	3.67	37.6
HGG + R2G (0.8M)	0.89	2.06	6.67	1.66	43.29	54.30	2.41	1.17	4.63	3.78	4.21

over time, these studies can effectively distinguish between dynamic and static quenching mechanisms. The fluorescence lifetime of fluorophore displays changes in case of dynamic quenching, while it remains constant in static quenching [31].

The fluorescence decay curve of HGG in phosphate buffer (pH 7.4) without and with different red 2G concentrations (0.4 and 0.8 × 10^{-4} mol L^{-1}), was examined at an excitation wavelength of 278 nm with emission maxima of 334 nm. The fluorescence lifetime decay curves were fitted with the exponential decay function as shown in Fig. 5. Moreover, the optimal model was obtained by fitting the tail with three exponentials and evaluating the goodness of the fits using the corresponding χ^2 values [32].

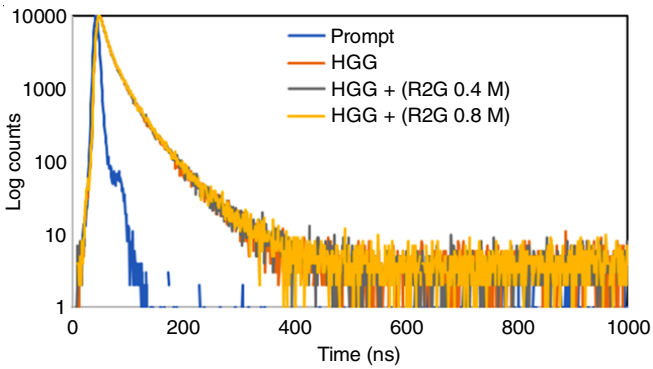

Fig. 5. Time-resolved fluorescence decays of human gamma globulin in phosphate buffer (pH = 7.4) with different concentrations of red 2G (1) 0.0, (2) 0.4 and (3) 0.8 × 10^{-4} M

To calculate the bi-exponential iterative mean lifetime, the following formula was utilized.

$$\langle \alpha \rangle = \frac{\propto_1 \tau_1^2 + \propto_2 \tau_2^2 + \propto_3 \tau_3^2}{\alpha_1\tau_1 + \alpha_2\tau_2 + \alpha_3\tau_3} \quad (4)$$

The average lifetime parameters of free HGG were calculated from the multiexponential fitting of the decay profiles and presented in Table-2. The calculated τ_{avg} for free HGG was found to be 1.77 ns. Interestingly, at two different R2G concentrations, the τ_{avg} changed to 1.67 and 1.66 ns. These results suggest that the system formation has minimal impact on the decay time of HGG, indicating the stability of the system. The fluorescence quenching of HGG caused by R2G was determined to be a static mechanism resulting from the formation of a ground-state R2G-HGG compound [24]. This conclusion was consistent with the fluorescence quenching inference.

FTIR studies: The conformational sensitivity of the protein's amide bands is primarily determined by the hydrogen bonding and coupling between transition dipoles [33,34]. The spectral region monitored in this study is shown in Fig. 6. The FTIR peak assignments of HGG with and without RED 2G are listed in Table-3.

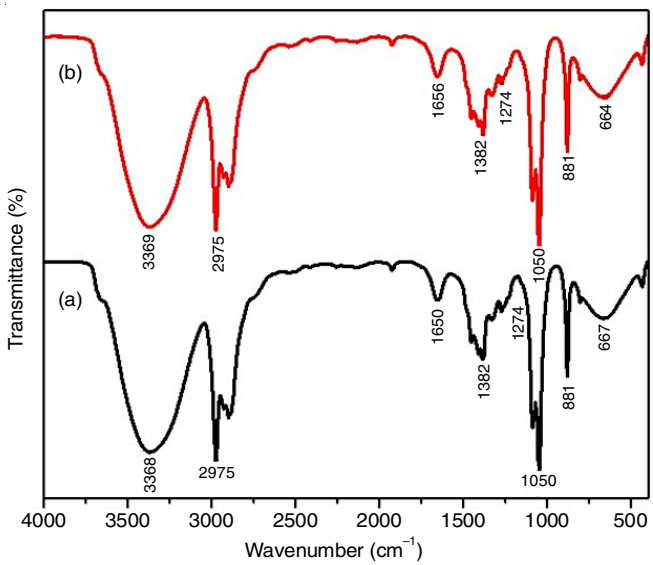

Fig. 6. FTIR spectra of (a) Human gamma globulin, (b) Human gamma globulin + red 2G

TABLE-3
FTIR TENTATIVE PEAK ASSIGNMENTS OF HGG WITHOUT AND WITH RED 2G DYE

Wavenumber (cm^{-1})		Tentavtive peak assignments
HGG	HGG + RED2G	
3368	3369	NH stretching
2975	2975	C–H antisymmetric and symmetric stretching
1650	1656	C=O stretching
1382	1382	N-H bending
1274	1274	N-H bending, C-N stretching
1050	1050	C–C and C–OH stretching modes
881	881	C–H bending vibration
667	664	OCN bending

The repeating units of protein, including polypeptides, produce nine distinctive IR absorption bands, namely amides A and B and amides I to VII. The most significant vibrational bands of the protein backbone are amides I, II and III [35]. The FTIR spectra of the HGG-R2G complex are similar to that of HGG protein indicating that there were no major changes in the protein structure as a result of complex formation. The absence of new spectrum signals during the binding process of HGG with R2G suggests that there were no new covalent bonds formed. The amide-I, which is situated between 1700

and 1600 cm^{-1} in the FTIR spectra study of HGG, reveals the secondary structure of HGG [36]. The C=O stretch band is mostly linked to the amide-I [37]. Changes in the secondary structure of HGG can be seen by examining the amide bands' peptide moiety frequencies. The FT-IR spectrometry analysis of the HGG and HGG-R2G complex revealed that the peak position of the amide-I band moved from 1650 (α-helix) to 1656 cm^{-1}, while the amide A band moved from 3368 cm^{-1} to 3369 cm^{-1}. There was a blue shift from 667 cm^{-1} to 664 cm^{-1} in the amide IV band of HGG upon interaction with R2G. The modifications made to the protein structural subunits' C=O and N-H, OCN groups were found to interact with R2G. The results indicated that R2G caused changes in the conformation of HGG during the binding process. The reduction in the intensity of the amide-I band suggested that R2G was the cause of instability in the α-helical structure of protein, which confirms that the secondary structure of HGG was affected [38].

Molecular docking: *In silico* docking predicts the optimal orientation of the ligand in the receptor's active site [39] and investigates the compatibility between a ligand and a protein target at the molecular level [40]. At the primary binding site of HGG, molecular docking has been carried out with R2G. The results are shown in Fig. 7 and Table-4.

About 450 amino acid residues make up the two heavy chains of HGG and 210-230 amino acid residues make up the two light chains. The analysis of the crystalline HGG's three-dimensional structure has demonstrated that the antigen-binding site is distributed over a 1.5 nm sized "shallow cavity" (cleft) that contains roughly 10-12 amino acid residues from the complement determinant region (CDR) of Fab. The semi-antigen can enter the cleft and attached itself to the CDR's amino acid residues through hydrogen bonds, van der Waals forces, electrostatic and hydrophobic interactions and other mechanisms [41].

TABLE-4
INTERACTING RESIDUES OF HUMAN GAMMA GLOBULIN WITH RED 2G DYE

Residues	Bond types	Distance (Å)
THR165	Hydrogen bond	2.78
GLU165	Hydrogen bond	1.94
GLU148	Hydrogen bond	1.72
VAL150	Hydrogen bond	1.90
VAL152	Hydrogen bond	2.47
THR165	Hydrogen bond	2.91
GLU165	Hydrogen bond	2.45
THR165	Hydrogen bond (carbon hydrogen bond)	3.43
HIS164	Hydrophobic (Pi-Pi T-shaped)	4.85
PRO167	Hydrophobic (Pi-alkyl)	5.09

Throughout the docking process, only a maximum of ten conformers were considered for the compound. For further analysis, the conformer with the lowest binding free energy (ΔG = -7.29 kcal/mo1) was utilized (Table-5). The interaction between R2G and the amino acid residues of HGG is through hydrogen bonds, as evident from Fig. 7. It was observed that the aromatic ring of R2G can form numerous hydrogen bonds with adjacent amino acid residues, including Thr-165, Glu-165, Glu-148, Val-150 and Val-152, to facilitate the formation

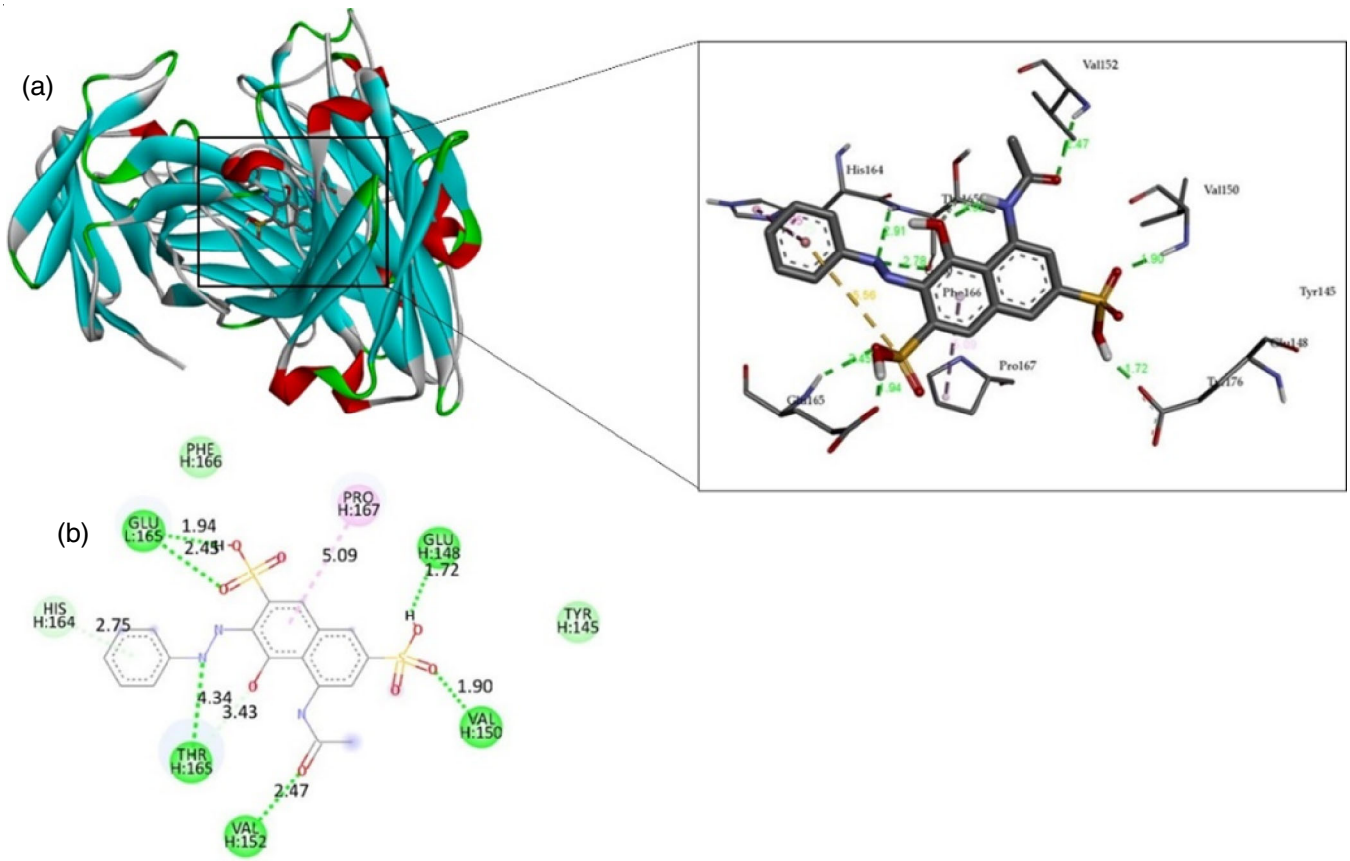

Fig. 7. (a) 3D Molecular docking, (b) 3D Ligand interaction and (c) 2D diagram ligand interaction of human gamma globulin with red 2G dye

TABLE-5
MOLECULAR DOCKING RESULTS OF HGG-R2G COMPLEX

Dye	Protein id	Binding energy (Kcal/mol)	RMSD (A)	Inhibition constant (Um)	Inter molecular energy (Kcal/mol)	vdw + Hbond + Desolv energy (Kcal/mol)	Electrostatic Energy (Kcal/mol)
R2G	1aj7	-7.29	21.74	4.53	-9.68	-9.66	-0.01

of a ligand-protein complex (Fig. 7c-d). Additionally, there exist hydrophobic interactions (pi-alkyl and pi-pi T-shaped) between red 2G, Pro-167 and His-164.

Moreover, the dye molecule may transfer energy and quench the fluorescence of HGG as it is close to the chromophore's Tyr 165 amino acid residue. The binding of ligands into the cavities of HGG is influenced by the hydrogen bonds and hydrophobic (pi-pi T-shaped and pi-alkyl) contacts. R2G has a stronger binding affinity to HGG due to the availability of the more hydrogen bonds [42,43].

Protein aggregation studies

Turbidity measurements: Measurements of the turbidity were performed to look into how the R2G affected the aggregation of HGG at pH 2. The aggregation in the HGG solutions was described using the turbidity at 650 nm because R2G absorbance is almost zero at this wavelength [44]. Fig. 8a shows the curve of turbidity at 650 nm against R2G concentrations.

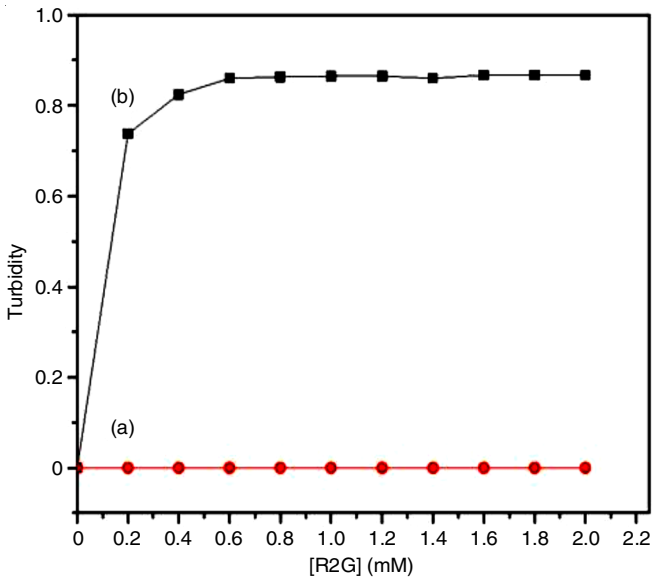

Fig. 8. Turbidity profile of (a) Red 2G alone without the addition of HGG (pH 2.0), (b) HGG with R2G dye (pH 2.0)

At pH 2, red 2G dye (Fig. 8a) dye does not exhibit any turbidity even in the absence of HGG indicating that the dye does not self-aggregate. The results of the experiment showed that pH has no effect on the aggregation of HGG (without R2G) as there was no turbidity observed at pH 2. However, when R2G was introduced, the turbidity increased. The amount of R2G added directly impacted the level of turbidity. At the concentration of 0.2 mM, the turbidity remained low, but as it increased to 0.4 mM, the turbidity began to increase. It peaked at 0.6 mM and remained constant until 2 mM R2G. Therefore, at pH 2.0, a concentration of 0.4 mM R2G is ideal for causing HGG proteins to aggregate. The aggregation kinetics of HGG protein did not follow the typical sigmoidal curve, which includes initial lag, growth and equilibrium phases. This suggests that the protein aggregation was not dependent on nuclei. Previous studies have shown that a sigmoidal curve indicates a nucleus-dependent phenomenon [45]. Interestingly the red 2G-induced aggregation did not display a lag phase and HGG was directly converted into larger aggregates. HGG has an isoelectric point (pI) of 7.2 [46,47], which is the least negatively charged among the serum proteins. When the pH of protein solution is lower than its isoelectric point (pI), the protein molecules acquire a net positive charge. This positive charge enables the protein to interact electrostatically with negatively charged species present in the surrounding solution.

The aggregation of HGG is caused by the interaction between the negatively charged sulphonic groups present in red 2G and the positively charged amino acid residues of HGG. R2G neutralizes the charges on HGG, which in turn leads to the aggregation of HGG. The neutralization of charge also perturbs the HGG-solvent interaction, favouring hydrophobic moieties at low pH, which then creates a suitable environment for HGG aggregation. Both electrostatic and hydrophobic interactions are involved in R2G-induced aggregation. This kind of interaction has been observed in other studies that investigate the impact of food colours on the aggregation of serum and globular proteins [48,49].

In conclusion, the experiment revealed that pH alone has no effect on HGG protein aggregation, but the presence of R2G at low pH can significantly increase turbidity. The concentration of R2G is crucial in determining the level of turbidity and at 0.4 mM, it can cause HGG proteins to aggregate.

Morphological studies: Protein aggregation morphology is an important factor in understanding the behaviour of proteins in solution. For this reason, FESEM imaging was used to visualize the morphology of protein aggregates. Specifically, the FESEM images of HGG at pH 2 were taken both before and after incubation with 1.8 mM of R2G at room temperature. The images were compared to gain a better understanding of the morphology of R2G-induced aggregates. Fig. 9a-b demonstrate the HGG's incubation with a range of red 2G concentration (1 mM) at room temperature and pH 2. At pH 2, the HGG protein reacts with 1.0 mM of R2G, resulting in the formation of precipitates which is clearly visible. The FESEM image of HGG without R2G does not show any aggregations, indicating that HGG does not self-aggregate.

Throughout the process, FESEM analysis detected the formation of fibrillar aggregates. Further, the electron micrographs showed that R2G caused the formation of spherical shaped aggregates with different diameters. The FESEM results indicated that these fibrillar and spherical aggregates were formed due to the interactions between R2G and other compounds involved in the process.

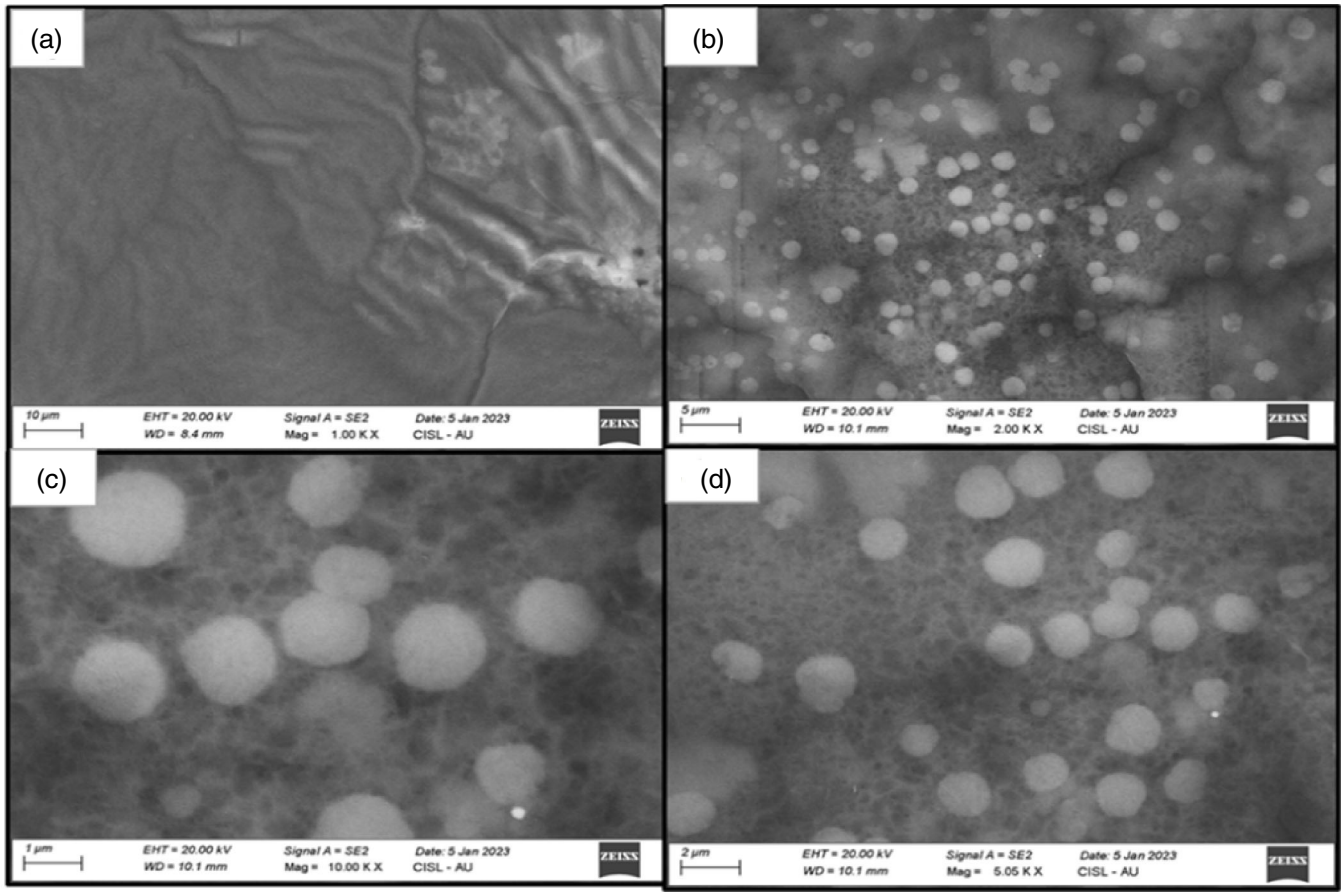

Fig. 9. (a) The HGG (0.2 mg mL^{-1}) without red 2G dye, (b) The HGG (0.2 mg mL^{-1}) was treated with 1.8 mM of red 2G dye at pH 3.5 for overnight incubation at 2.00 Kx magnification, (c) 5.00 Kx magnification

Cytotoxicity of red 2G in THP1 cell lines: With regard to THP1 cell lines, the study sought to determine whether the red 2G dye would have any cytotoxic effects [50]. This cell line was chosen due to the likelihood of the dye's exposure through food ingestion, which can enter the bloodstream [51].

The MTT assay was conducted after 48 h of incubation to determine the cell viability. The results showed that R2G dye exhibited a concentration-dependent cytotoxic effect on the cells as revealed by the assay (Figs. 10). The impact of R2G on THp1 cell proliferation revealed that R2G did not have a significant effect on cell viability at low concentrations. Nonetheless, in contrast to the control group, a concentration of 2000 µg/mL led to a significant reduction in the cell viability. This concentration can be considered as the threshold concentration for toxicity. Moreover, at a concentration of 2500 µg/mL, R2G was found to be highly toxic and caused a drastic decline in the quantity of viable cells, destroying 81% of the cells at a concentration of 2500 µg/mL.

Further analysis revealed that the concentration needed to suppress cell viability by 50% was 1475.8 µg/mL, determined using an equation $y = 0.0302x + 94.571$ with $R^2 = 0.999$ (Fig. 11). The azo dye was observed to be inhibiting the growth of THP1 cells at all concentrations.

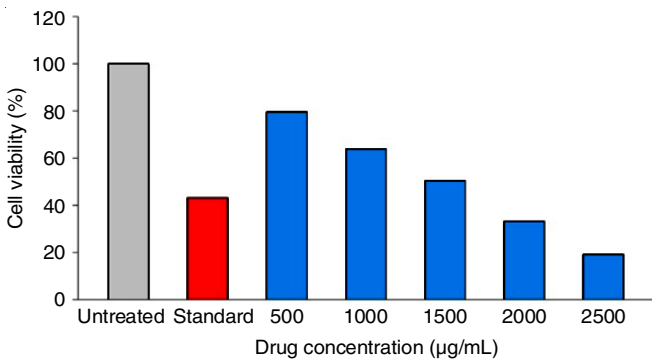

Fig. 10. Percentage of viability of THP-1 cells was determined *via* MTT assay upon exposure to varying concentrations of red 2G

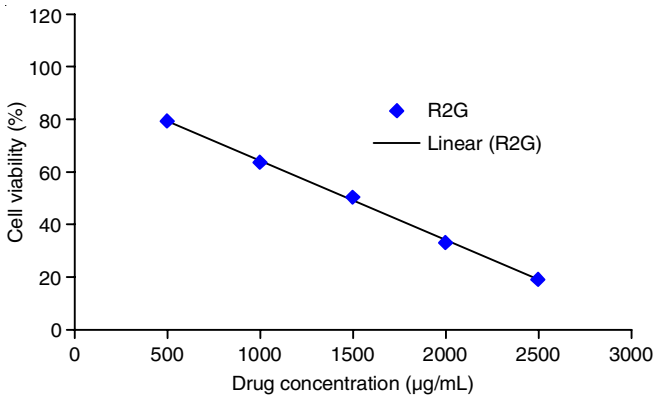

Fig. 11. IC_{50} curve of THP-1 cells exposed to varying concentrations of red 2G, as measured by MTT assay

In order to verify the cell viability data, the morphology of THp1 cells was examined after being exposed to R2G at the concentrations ranging from 500 to 2500 µg/mL (Fig. 12). Results showed that R2G exposure caused cell death in a dose-dependent manner. Cells in the control group displayed healthy, normal morphology and were properly attached to the surface. However, cells in the treated groups showed irregular morphology, floated in the culture medium and had a lower cell density with a significant number of dead cells. These findings suggest that R2G can potentially cause cytotoxicity in THP1 cells in a dose-dependent manner. Therefore, this *in vitro* study analyzed the differences in the ability of RED 2G to produce toxicity upon exposure to human monocytes, THP-1. The obtained results showed a significant difference between the cell viability of RED 2G-treated cells and the negative control, indicating cytotoxicity. Furthermore, the closeness of the results to the positive control suggests an even higher level of cytotoxicity.

Conclusion

The successful characterization of the binding interactions between the synthetic red 2G dye and human gamma globulin (HGG) has been discussed. Insight into the static quenching mechanism was provided by the quenching constant and stability data. The binding constant revealed a hydrophobic interaction-based static quenching mechanism. The results from synchronous fluorescence and FTIR spectroscopies showed that R2G caused structural changes in protein HGG. Autodock-based molecular docking studies revealed that R2G binds with HGG with greater binding affinity and also indicated the likely binding site of TART. Turbidity and FESEM results showed that the R2G dye induces amyloid-like aggregates at pH 2 due to the electrostatic and hydrophobic interactions. The cytotoxicity of the dye was also investigated using a human monocyte cell line, THP-1 (floating cells), for a range of concentrations (500-2500 µg/mL) and incubation time (48 h). The results indicated that the dye exhibited more toxicity at higher concentrations in THP-1 cells. These studies provides the comprehensive analysis of the energetics of the food colorants red 2G interaction with HGG. The results of this research provide the crucial insights into the toxicological effects of red 2G dye and can potentially advance further research on the usage of synthetic colourants in food products.

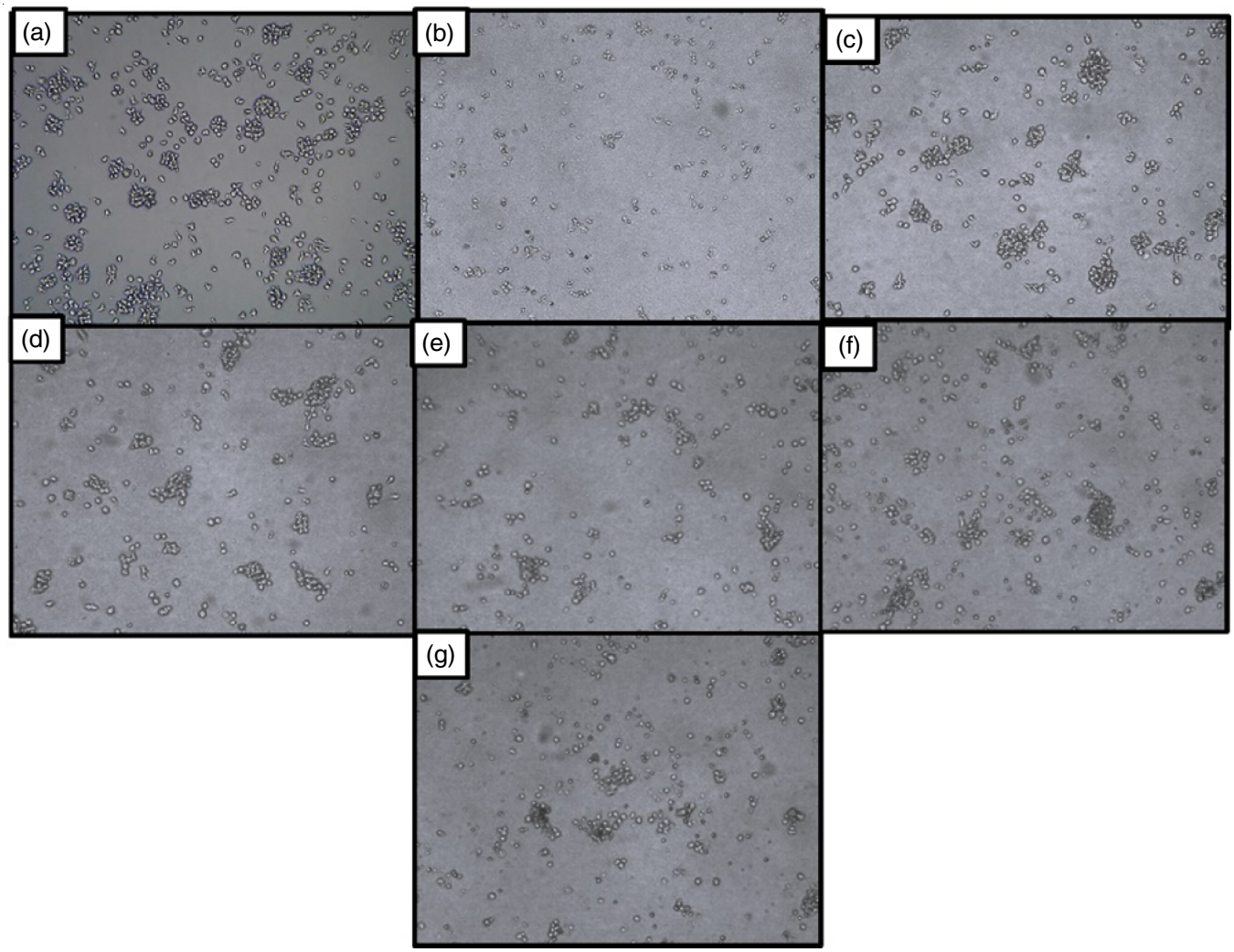

Fig. 12. Morphological images of (a) untreated, (b) positive control and treated THP-1 cells with different concentrations of red 2G (c) 500 µg/mL, (d) 1000 µg/mL, (e) 1500 µg/mL, (f) 2000 µg/mL, (g) 2500 µg/mL

CONFLICT OF INTEREST

The authors declare that there is no conflict of interests regarding the publication of this article.

REFERENCES

1. J. Cunha-Vaz, R. Bernardes and C. Lobo, *Eur. J. Ophthalmol.*, **21(Suppl 6)**, 3 (2011); https://doi.org/10.5301/EJO.2010.6049
2. Y. Guo, H. Lee and H. Jeong, Eds.: A. Blanco and G. Blanco, Proteins, In: Medical Biochemistry, Academic Press, Chap. 3, pp. 21-71 (2020); https://doi.org/10.1016/bs.pmbts.2020.04.002
3. T. Tripathi, S. Saxena, S. Saha, J. Saxena, D. Rastogi, C. Srivastava and P. Kanowjia, *Int. J. Physiol.*, **8**, 80 (2020).
4. J.S. Marshall, R. Warrington, W. Watson and H.L. Kim, *Allergy Asthma Clin. Immunol.*, **14(Suppl 2)**, 49 (2018); https://doi.org/10.1186/s13223-018-0278-1
5. K.B. Megha and P.V. Mohanan, *Int. J. Biol. Macromol.*, **169**, 28 (2021); https://doi.org/10.1016/j.ijbiomac.2020.12.073
6. J.A. Hooper, *LymphoSign J.*, **2**, 181 (2015); https://doi.org/10.14785/lpsn-2014-0025
7. R.I. Alsantali, Q.A. Raja, A.Y.A. Alzahrani, A. Sadiq, N. Naeem, E.U. Mughal, M.M. Al-Rooqi, N. El-Guesmi, Z. Moussa and S.A. Ahmed, *Dyes Pigm.*, **199**, 110050 (2022); https://doi.org/10.1016/j.dyepig.2021.110050
8. S. Benkhaya, S. M'rabet and A. El Harfi, *Heliyon*, **6**, e03271 (2020); https://doi.org/10.1016/j.heliyon.2020.e03271
9. M. Asif Ahmed, A.S. Al-Khalifa, D.M. Al-Nouri and M.F.S. El-din, *Saudi J. Biol. Sci.*, **28**, 27 (2021); https://doi.org/10.1016/j.sjbs.2020.08.025
10. H. Sun, Y. Yao, F. Wei, Q. Zhao, B. Liu and L. Zhang, *Turk. J. Chem.*, **45**, 5 (2021); https://doi.org/10.3906/kim-2002-10
11. R.B. Haveland-Smith, R.D. Combes and B.A. Bridges, *Mutat. Res.*, **64**, 241 (1979); https://doi.org/10.1016/0165-1161(79)90093-1
12. S. Kamaljeet, S. Bansal and U. SenGupta, *Front Chem.*, **4**, 00050 (2017); https://doi.org/10.3389/fchem.2016.00050
13. D.L. Mobley and K.A. Dill, *Structure*, **17**, 489 (2009); https://doi.org/10.1016/j.str.2009.02.010
14. S. Moradi, M. Shahlaei, F. Balaei, M. Ansari and N. Farhadian, *Res. Pharm. Sci.*, **16**, 58 (2021); https://doi.org/10.4103/1735-5362.305189
15. S.A. Alex, N. Chandrasekaran and A. Mukherjee, *IET Nanobiotechnol.*, **13**, 522 (2019); https://doi.org/10.1049/iet-nbt.2018.5408
16. K. Baranowska, M. Moñka, P. Bojarski and M. Józefowicz, *Int. J. Mol. Sci.*, **22**, 11705 (2021); https://doi.org/10.3390/ijms222111705
17. J. Lin, W. Hua, Y. Zhang, C. Li, W. Xue, J. Yin, Z. Liu and X. Qiu, *Biochim. Biophys. Acta Gen.*, **1850**, 419 (2015); https://doi.org/10.1016/j.bbagen.2014.11.016
18. S. Bakkialakshmi and D. Chandrakala, *Spectrochim. Acta A Mol. Biomol. Spectrosc.*, **88**, 2 (2012); https://doi.org/10.1016/j.saa.2011.10.076
19. Y. Liu, W. He, W. Gao, Z. Hu and X. Chen, *Int. J. Biol. Macromol.*, **37**, 1 (2005); https://doi.org/10.1016/j.ijbiomac.2005.04.005
20. O.A. Chaves, A.P.D.O. Amorim, L.H. Castro, C.M.R. Sant'Anna, M.C. De Oliveira, D. Cesarin-Sobrinho, J.C. Netto-Ferreira and A.B. Ferreira, *Molecules*, **20**, 19526 (2015); https://doi.org/10.3390/molecules201019526
21. P. Sadatmousavi, E. Kovalenko and P. Chen, *Langmuir*, **30**, 11122 (2014); https://doi.org/10.1021/la502422u
22. A. Sharma, K.S. Ghosh, B.P. Singh and A.K. Gathania, *Methods Appl. Fluoresc.*, **3**, 025002 (2015); https://doi.org/10.1088/2050-6120/3/2/025002
23. A.A. Salem, M. Lotfy, A. Amin and M.A. Ghattas, *Biochem. Biophys. Rep.*, **20**, 100670 (2019); https://doi.org/10.1016/j.bbrep.2019.100670
24. X. Li, X. Wang, H. Liu, Y. Peng, Y. Yan and T. Ni, *J. Mol. Struct.*, **1225**, 129291 (2021); https://doi.org/10.1016/j.molstruc.2020.129291
25. X. Su, L. Wang, Y. Xu, L. Dong and H. Lu, *Ecotoxicol. Environ. Saf.*, **207**, 111280 (2021); https://doi.org/10.1016/j.ecoenv.2020.111280
26. E. Lissi, C. Calderón and A. Campos, *Photochem. Photobiol.*, **89**, 1413 (2013); https://doi.org/10.1111/php.12112
27. H. Zhang, R. Cai, C. Chen, L. Gao, P. Ding, L. Dai and B. Chi, *Int. J. Mol. Sci.*, **24**, 13281 (2023); https://doi.org/10.3390/ijms241713281
28. S. Bakkialakshmi and D. Chandrakala, *J. Mol. Liq.*, **168**, 1 (2012); https://doi.org/10.1016/j.molliq.2012.01.018
29. J. Xu, Y. Huang, Y. Wei, X. Weng and X. Wei, *Foods*, **12**, 1637 (2023); https://doi.org/10.3390/foods12081637
30. Y. Chen, M. Li, J. Kong, J. Liu and Q. Zhang, *Foods*, **12**, 1561 (2023); https://doi.org/10.3390/foods12081561
31. K.A. Paterson, J. Arlt and A.C. Jones, *Methods Appl. Fluoresc.*, **8**, 025002 (2020); https://doi.org/10.1088/2050-6120/ab71c3
32. J.R. Albani, *J. Fluoresc.*, **24**, 105 (2014); https://doi.org/10.1007/s10895-013-1274-y
33. T.K. Maiti, K.S. Ghosh and S. Dasgupta, *Proteins*, **64**, 355 (2006); https://doi.org/10.1002/prot.20995
34. S. Suwal, A. Doyen and L. Bazinet, *J. Membr. Sci.*, **496**, 267 (2015); https://doi.org/10.1016/j.memsci.2015.08.056
35. J. Bandekar and S. Krimm, *Proc. Natl. Acad. Sci. USA*, **76**, 774 (1979); https://doi.org/10.1073/pnas.76.2.774
36. A. Sadat and I.J. Joye, *Appl. Sci.*, **10**, 5918 (2020); https://doi.org/10.3390/app10175918
37. F. Mallamace, C. Corsaro, D. Mallamace, S. Vasi, C. Vasi and G. Dugo, *Comput. Struct. Biotechnol. J.*, **13**, 33 (2015); https://doi.org/10.1016/j.csbj.2014.11.007
38. A. Basu and G.S. Kumar, *J. Hazard. Mater.*, **289**, 204 (2015); https://doi.org/10.1016/j.jhazmat.2015.02.044
39. M. Gupta, R. Sharma and A. Kumar, *Comput. Biol. Chem.*, **76**, 210 (2018); https://doi.org/10.1016/j.compbiolchem.2018.06.005
40. X. Li and T. Ni, *J. Biol. Phys.*, **42**, 415 (2016); https://doi.org/10.1007/s10867-016-9415-6
41. L. Ying, W. Chao and L. Guanghua, *J. Mol. Struct.*, **980**, 108 (2010); https://doi.org/10.1016/j.molstruc.2010.06.044
42. Y. Liu, R. Lei, Z. Hu, X. Chen, F. Shen and J. Jing, *Spectrosc. Lett.*, **39**, 265 (2006); https://doi.org/10.1080/00387010600636999
43. Y. Liu, Z. Yang, J. Du, X. Yao, R. Lei, X. Zheng, J. Liu, H. Hu and H. Li, *Immunobiology*, **213**, 651 (2008); https://doi.org/10.1016/j.imbio.2008.02.003
44. N.K. Daud and B.H. Hameed, *J. Hazard. Mater.*, **176**, 938 (2010); https://doi.org/10.1016/j.jhazmat.2009.11.130
45. Z.L. Almeida and R.M. Brito, *Molecules*, **25**, 1195 (2020); https://doi.org/10.3390/molecules25051195
46. E.C. Franklin and F. Prelli, *J. Clin. Invest.*, **39**, 1933 (1960); https://doi.org/10.1172/JCI104218
47. A. Higuchi, S. Mishima and T. Nakagawa, *J. Membr. Sci.*, **57**, 175 (1991); https://doi.org/10.1016/S0376-7388(00)80677-8
48. N.A. Al-Shabib, J.M. Khan, M.A. Alsenaidy, A.M. Alsenaidy, M.S. Khan, F.M. Husain, M.R. Khan, M. Naseem, P. Sen, P. Alam and R.H. Khan, *Spectrochim. Acta A Mol. Biomol. Spectrosc.*, **191**, 116 (2018); https://doi.org/10.1016/j.saa.2017.09.062
49. N.A. Al-Shabib, J.M. Khan, M.S. Khan, M.S. Ali, A.M. Al-Senaidy, M.A. Alsenaidy, F.M. Husain and H.A. Al-Lohedan, *Int. J. Biol. Macromol.*, **98**, 277 (2017); https://doi.org/10.1016/j.ijbiomac.2017.01.097
50. W. Chanput, J.J. Mes and H.J. Wichers, *Int. Immunopharmacol.*, **23**, 37 (2014); https://doi.org/10.1016/j.intimp.2014.08.002
51. T.L. Heil, K.R. Volkmann, J.C. Wataha and P.E. Lockwood, *J. Oral Rehabil.*, **29**, 401 (2002); https://doi.org/10.1046/j.1365-2842.2002.00893.x